Neuron, Vol. 48, 797–809, December 8, 2005, Copyright ©2005 by Elsevier Inc. DOI 10.1016/j.neuron.2005.09.015

Development of Precise Maps in Visual Cortex Requires Patterned Spontaneous Activity in the Retina

Jianhua Cang,[1] René C. Rentería,[2] Megumi Kaneko,[1] Xiaorong Liu,[2] David R. Copenhagen,[2] and Michael P. Stryker[1,*]
[1] W. M. Keck Foundation Center for Integrative Neuroscience
Department of Physiology
[2] Departments of Ophthalmology and Physiology
University of California, San Francisco
San Francisco, California 94143

Summary

The visual cortex is organized into retinotopic maps that preserve an orderly representation of the visual world, achieved by topographically precise inputs from the lateral geniculate nucleus. We show here that geniculocortical mapping is imprecise when the waves of spontaneous activity in the retina during the first postnatal week are disrupted genetically. This anatomical mapping defect is present by postnatal day 8 and has functional consequences, as revealed by optical imaging and microelectrode recording in adults. Pharmacological disruption of these retinal waves during the first week phenocopies the mapping defect, confirming both the site and the timing of the disruption in neural activity responsible for the defect. Analysis shows that the geniculocortical miswiring is not a trivial or necessary consequence of the retinogeniculate defect. Our findings demonstrate that disrupting early spontaneous activity in the eye alters thalamic connections to the cortex.

Introduction

A fundamental feature of mammalian cortical organization is that the receptive fields (RFs) of cortical neurons are organized into topographic maps. Such an arrangement of RFs results from topographically precise wiring of connections between thalamic and cortical neurons. In the visual system, for example, neighboring neurons in the retina project their axons to neighboring neurons in the dorsal lateral geniculate nucleus (dLGN), which, in turn, project to neighboring targets in the primary visual cortex (V1), thus preserving a continuous retinotopic representation of the visual world. While most studies have focused on retinotopic mapping of retinal axons to their subcortical targets (Eglen et al., 2003; McLaughlin et al., 2003a), how the precise mapping of geniculocortical projections is achieved during development is not well understood.

Spontaneous neuronal activity has been shown to play an important role in the formation and maturation of neural circuits (Katz and Shatz, 1996). In the visual system, waves of action potentials propagate across retinal ganglion cells before the eyes open (Galli and Maffei, 1988; Meister et al., 1991; Wong et al., 1993). Many studies have shown that such patterned activity in the developing retina is required for the refinement of retinal projections to their subcortical targets (Chandrasekaran et al., 2005; Grubb et al., 2003; McLaughlin et al., 2003b; Mrsic-Flogel et al., 2005; Muir-Robinson et al., 2002; Penn et al., 1998; Shatz and Stryker, 1988; but see Huberman et al., 2003). However, the role of retinal waves in mapping geniculocortical projections has remained an open question. While complete blockade of retinal activity can disrupt the segregation of geniculocortical axons into ocular dominance columns (ODCs) (Stryker and Harris, 1986), experiments using enucleation suggest that retinal input may not be needed for ODC formation (Crowley and Katz, 1999) and that molecular cues or activity patterns within the geniculocortical pathway are sufficient for patterning ODCs (Miller et al., 1989). Indeed, correlated spontaneous activity is present in the dLGN and V1 before vision onset and in the absence of retinal input (Chiu and Weliky, 2001; Weliky and Katz, 1999). However, the temporal properties of the spontaneous activity in the dLGN and V1 are altered by severing retinal inputs (Chiu and Weliky, 2001; Weliky and Katz, 1999). The temporal pattern of correlated spontaneous activity may be critical for driving fine-scale retinotopic mapping along the visual pathway (Butts and Rokhsar, 2001).

To address whether patterned spontaneous activity in the retina is required for the precise mapping of geniculocortical projections, we studied a mutant mouse line that has uncorrelated retinal activity during development due to the deletion of the β2 subunit of the nicotinic acetylcholine receptor (nAChR) (Xu et al., 1999). As in other mammals, the early retinal waves in mice are mediated by cholinergic transmission (Bansal et al., 2000; Feller et al., 1996). Deleting the β2 subunit of the nAChR disrupts the patterns of retinal activity only during the first postnatal week (Bansal et al., 2000; Grubb et al., 2003), when retinotopic maps are being established and refined in the dLGN (Godement et al., 1984) and visual cortex (Lund and Mustari, 1977); the spontaneous waves of retinal activity return to normal in the second week. Rossi et al. have shown that the $\beta2^{-/-}$ mouse visual system has decreased spatial resolution for grating stimuli at the cortical level, but not in the retina (Rossi et al., 2001), indicating a postretinal defect in the visual pathways. Indeed, recent physiological recordings have shown that fine-scale retinotopic mapping of retinogeniculate projections is defective in the nasotemporal visual axis in $\beta2^{-/-}$ mice (Grubb et al., 2003), although the polarity of the map and individual RFs are grossly normal (Grubb et al., 2003; Grubb and Thompson, 2004). It has remained unknown whether the absence of retinal waves affects precise, point-to-point, mapping of connections to the cortex in these mice.

In this study, we found that the anatomical mapping of geniculocortical projections is imprecise in the $\beta2^{-/-}$ mouse. Using optical imaging and microelectrode recording, we have demonstrated that cortical retinotopic maps of the $\beta2^{-/-}$ mouse are functionally defective, much more so than subcortical retinotopic maps. We

*Correspondence: stryker@phy.ucsf.edu

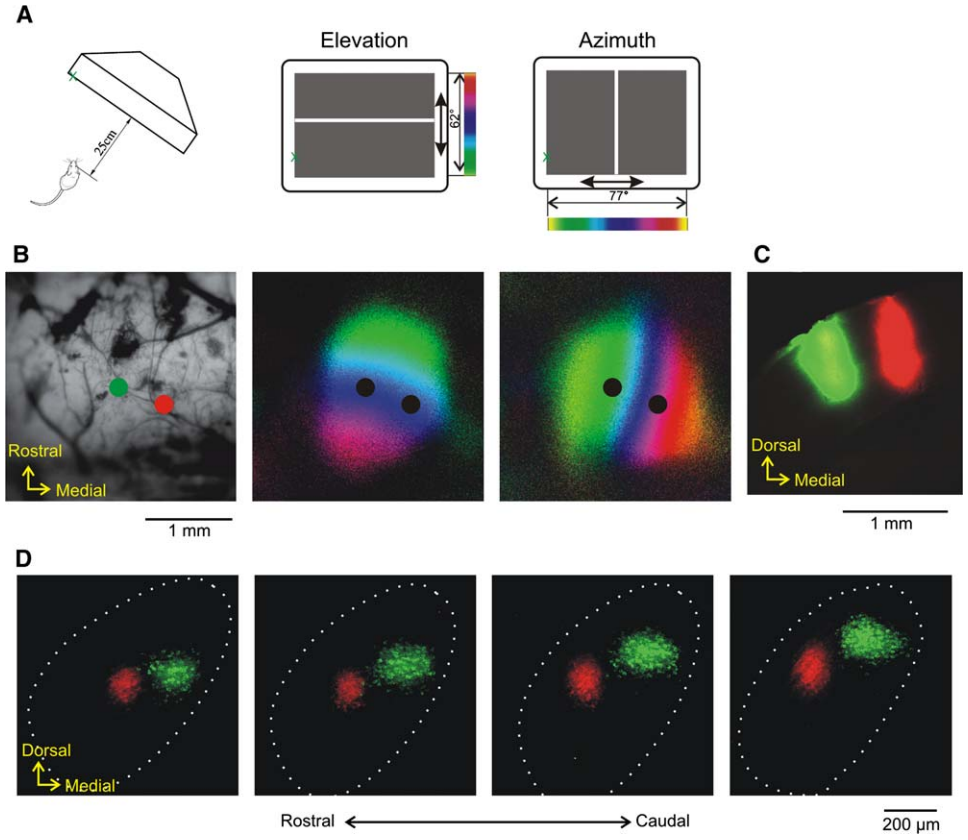

Figure 1. Topographically Precise Mapping of Geniculocortical Projections in WT Mice

(A) Visual stimuli used to assess cortical retinotopy. The monitor was placed as indicated in the left panel, contralateral to the hemisphere under study. Stimuli were thin moving bars (middle and right panels). Elevation and azimuth maps were obtained by stimulating the animal with bars moving vertically and horizontally, respectively. The position on the monitor that drove each site on the cortex is color-coded, as shown next to the monitors in the middle and right panels.

(B) Cortical vasculature pattern in the region being imaged and retinotopic maps of a WT mouse. The two colored dots indicate the locations where retrograde markers of corresponding colors were injected under the guidance of functional retinotopic maps. In the maps, the position of the visual field is represented by color according to the color scales in (A), and the response magnitude, by lightness.

(C) A coronal section of the injection sites.

(D) Retrogradely labeled neurons in the dLGN of this mouse. Four continuous coronal sections (100 μm thick) from rostral (left) to caudal (right) are shown. Dotted lines mark the border of the dLGN.

then altered the retinal activity in wild-type mice pharmacologically during the first week and phenocopied the mapping defect of geniculocortical projections, thereby confirming both the site and the timing of the disruption in neural activity. Finally, we found that the abnormal patterns of geniculocortical projections are present by postnatal day 8 (P8) and that removing the eyes afterwards has no effect on the projection patterns. These results establish a role for retinal waves in the fine-scale mapping of geniculocortical projections and indicate that a transient disturbance of neural activity in the sensory periphery has long-term consequences for the thalamocortical circuits.

Results

Topographically Precise Mapping of Geniculocortical Projections Is Defective in $\beta2^{-/-}$ Mice

As in other mammals, the primary visual cortex (V1) of the mouse is organized in a retinotopic manner. The cortical retinotopic maps can be revealed by optical imaging of intrinsic signals (Kalatsky and Stryker, 2003). Under the guidance of these functional maps of the visual cortex (Figure 1), we examined the anatomical mapping of geniculocortical projections by labeling dLGN neurons retrogradely with dye injection at defined topographic locations within V1. Injections of the retrograde marker cholera toxin subunit B (CTB) in V1 of adult wild-type (WT) mice revealed columns of labeled geniculate cells along the lines of projection. In coronal sections of the dLGN, labeled neurons form distinct clusters (Figure 1D).

The same tracing experiments were performed in β2 homozygous ($\beta2^{-/-}$) and heterozygous ($\beta2^{+/-}$) mice. In $\beta2^{+/-}$ mice, injections of the retrograde marker resulted in a labeling pattern similar to that in the WTs (Figure 2A and Figure S1; the latter is in the Supplemental Data available with this article online). In the $\beta2^{-/-}$ mice, however, the labeling patterns were quite different: similarly sized injections resulted in significantly larger labeled areas (Figure 2B and Figure S2). Furthermore, injection of two different colors of dyes at sites 500 μm apart in the visual cortex resulted in overlap between the two

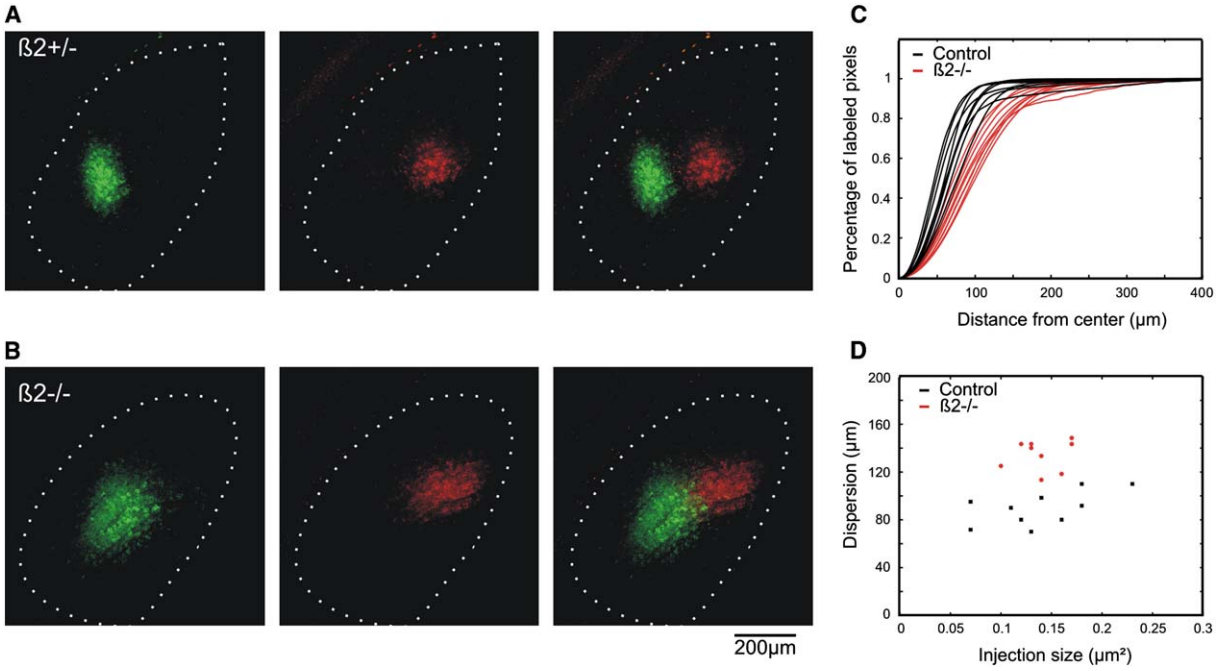

Figure 2. Point-to-Point Mapping of Geniculocortical Projection Is Imprecise in $\beta2^{-/-}$ Mice

(A) Retrogradely labeled neurons in the dLGN of a $\beta2^{+/-}$ mouse. Green neurons (left panel), red neurons (middle), and overlay of the two (right) are shown.

(B) Retrogradely labeled geniculate neurons at a similar level of a coronal section in a $\beta2^{-/-}$ mouse. Note the larger labeled areas and overlap of the two colors in the $\beta2^{-/-}$ dLGN compared to those in the $\beta2^{+/-}$.

(C) Quantification of retrogradely labeled areas in the dLGN. The percentage of labeled pixels was plotted as a function of the distance from the center of all of the labeled pixels. Each curve represents the average of one animal, with black curves from controls (both WTs and $\beta2^{+/-}$) and red curves from $\beta2^{-/-}$. Clear separation between controls and $\beta2^{-/-}$ is evident.

(D) The dispersion, the distance within which 80% of the labeled pixels are included, is plotted against the size of the injection site. The injections in the $\beta2^{-/-}$ mice were similar in size to those in the controls, and labeled areas in the dLGN were significantly larger ($p < 0.0001$) in $\beta2^{-/-}$ mice (134 ± 4µm) compared with those in the controls (90 ± 5µm).

colors in the $\beta2^{-/-}$ dLGN, but not in the $\beta2^{+/-}$ dLGN, indicating that near-neighbor dLGN neurons projected to a wider area in V1. We quantified the size of labeled areas in the dLGN by computing the percentage of labeled pixels as a function of the distance from the center of the labeled clusters (see Experimental Procedures). These plots are shown in Figure 2C for all injections in control (WT and $\beta2^{+/-}$, n = 10) and $\beta2^{-/-}$ mice (n = 9). Clear separation between the curves of control and those of $\beta2^{-/-}$ mice is evident. We measured the dispersion as the distance within which 80% of the labeled pixels were included: 90 ± 5 µm in control mice and 134 ± 4 µm in $\beta2^{-/-}$ mice ($p < 0.0001$). The difference between labeled areas in $\beta2^{-/-}$ and control mice was not due to a difference in injection sizes (control: 0.14 ± 0.02 mm^2; $\beta2^{-/-}$: 0.14 ± 0.01 mm^2; p = 0.81). For any given injection size, the labeled area was always bigger for the $\beta2^{-/-}$ mice (Figure 2D). Therefore, the mapping precision of geniculocortical projections is degraded in $\beta2^{-/-}$ mice. Interestingly, this mapping defect was especially severe in the nasotemporal visual axis (azimuth). The labeled pixels in the $\beta2^{-/-}$ were more spread out along the axis connecting the centers of the two clusters when the cortical injections were made at the same elevation and different azimuth (Figure 2 and Figures S1 and S2). When the tracer injections were made at different elevations along the same azimuth (Figure S3), the labeled pixels were still more spread out along the azimuth axis, which in this case is orthogonal to the line connecting the two clusters.

Precise Receptive Field Organization of Cortical Neurons Is Defective in $\beta2^{-/-}$ Mice

Recent physiological recordings in $\beta2^{-/-}$ mice have shown that fine-scale retinotopic mapping of retinogeniculate projections is degraded in the nasotemporal visual axis (Grubb et al., 2003). It is thus possible that the apparently imprecise anatomical mapping of geniculocortical projections in the $\beta2^{-/-}$ mice observed above might represent a compensation for the retinogeniculate defect, achieved by the convergence of the axons of all of the dispersed dLGN neurons that receive inputs from the same region of the retina onto each cortical target. In this scenario, the $\beta2^{-/-}$ mice would have normal functional maps in the cortex because the retinogeniculate defect is corrected by geniculocortical rewiring. Therefore, we examined the functional cortical maps, using optical imaging and microelectrode recording.

Examples of cortical retinotopic maps of a $\beta2^{+/-}$ and a $\beta2^{-/-}$ mouse are shown in Figure 3, in which the cortical retinotopy and response amplitude are plotted separately. There are clear differences between these maps. First, the response magnitude in the $\beta2^{-/-}$ maps was much weaker than that of the $\beta2^{+/-}$ mouse. The defect was especially severe for the azimuth maps. Second,

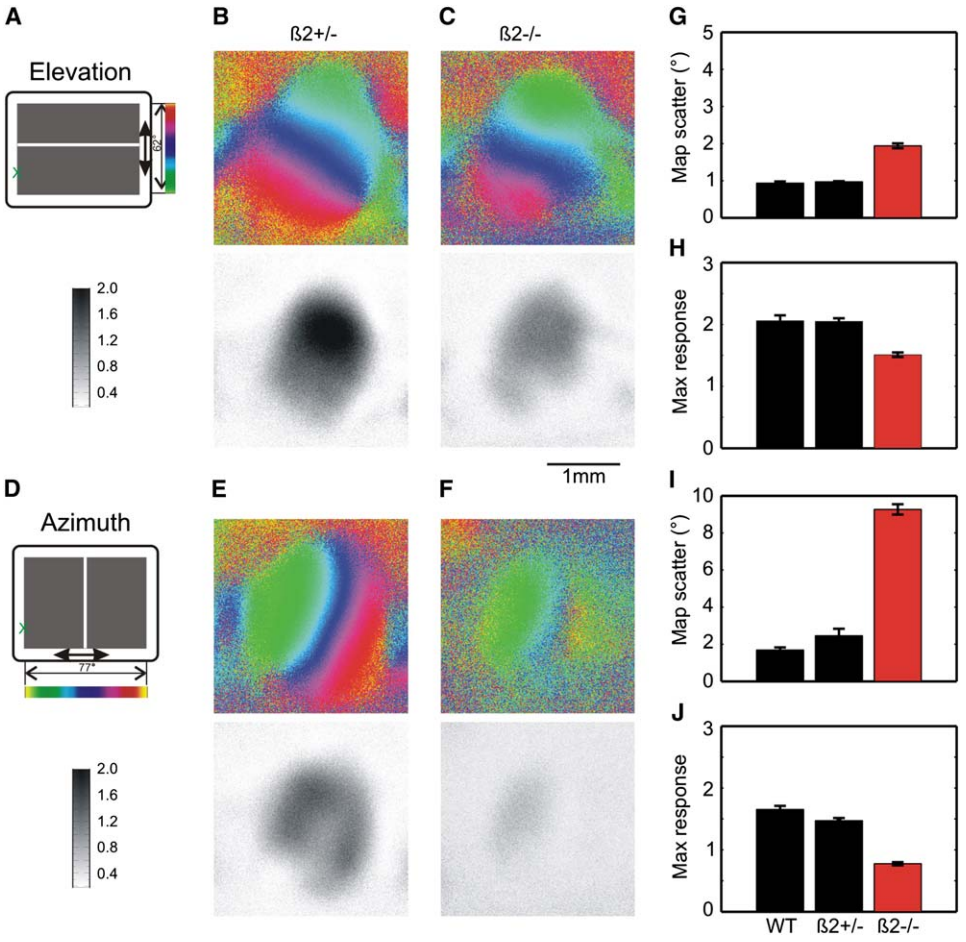

Figure 3. Cortical Retinotopic Maps Are Defective in $\beta2^{-/-}$ Mice

(A) Color code used to represent positions of different elevation lines on the stimulus monitor (top panel) and gray scale for response amplitude as fractional change in reflection $\times 10^4$ (bottom panel).

(B) Elevation map of a $\beta2^{+/-}$ mouse. Both retinotopy (top panel) and response magnitude (bottom panel) are shown.

(C) Elevation map of a $\beta2^{-/-}$ mouse.

(D) The color code and gray scale for plotting azimuth maps.

(E and F) Azimuth maps of the $\beta2^{+/-}$ and the $\beta2^{-/-}$ mouse. Note that the $\beta2^{-/-}$ retinotopy is more scattered and the response magnitude is weaker compared to those seen in the maps of $\beta2^{+/-}$.

(G–J) Quantification of cortical map defects in $\beta2^{-/-}$ mice. Compared to those of WT mice (n = 6), the $\beta2^{+/-}$ cortical maps (n = 5) are normal in terms of map quality (panels G and I: p = 0.77 for elevation; p = 0.38 for azimuth) and magnitude (panels H and J: p = 0.97 for elevation; p = 0.35 for azimuth). In contrast, the cortical maps of $\beta2^{-/-}$ (n = 14) are of lower quality (p < 0. 05 for elevation; p < 0.001 for azimuth) and weaker (p < 0.05 for elevation; p < 0.0001 for azimuth). Error bars represent the mean ± SEM.

in the $\beta2^{-/-}$ maps, the smooth progression of visual field location was more scattered or almost absent. These observations were confirmed by the quantitative analysis (Figure 3). $\beta2^{+/-}$ mice (n = 5) have normal cortical retinotopic maps in terms of response magnitude (p = 0.97 for elevation; p = 0.35 for azimuth) and map quality (p = 0.77 for elevation; p = 0.38 for azimuth. See the Experimental Procedures for details of calculating map quality). In contrast, the cortical maps of $\beta2^{-/-}$ mice (n = 14) are significantly weaker (p < 0.05 for elevation; p < 0.0001 for azimuth) and have lower quality (p < 0.05 for elevation; p < 0.001 for azimuth) compared to those of WTs (n = 6).

To confirm that the defective cortical maps in $\beta2^{-/-}$ mice revealed by intrinsic signal imaging resulted from poor retinotopic organization of cortical cells, we examined the receptive field (RF) organization of cortical neurons with multiunit recording using microelectrodes. In radial penetrations of visual cortex, the RF positions of multiunit recording sites were determined from their responses to horizontal or vertical bars sweeping across the stimulus monitor (Figures 4A–4C). The RF deviation of every recording site from the mean RF location of a given radial penetration provides a sensitive measure of the precision of cortical retinotopic organization. In $\beta2^{+/-}$ mice, the deviation of the RF location from the mean RF location is very small (1.6° ± 0.1°, n = 119 for elevation; 1.8° ± 0.1°, n = 117 for azimuth, three to seven sites per penetration). In contrast, $\beta2^{-/-}$ mice show much larger deviations (2.2° ± 0.2°, n = 164 for elevation; 3.5° ± 0.2°, n = 142 for azimuth). These differences were statistically significant for both elevation (p < 0.01) and azimuth (p < 0.0001), indicating that the RF structure is less precisely organized in the $\beta2^{-/-}$ mice.

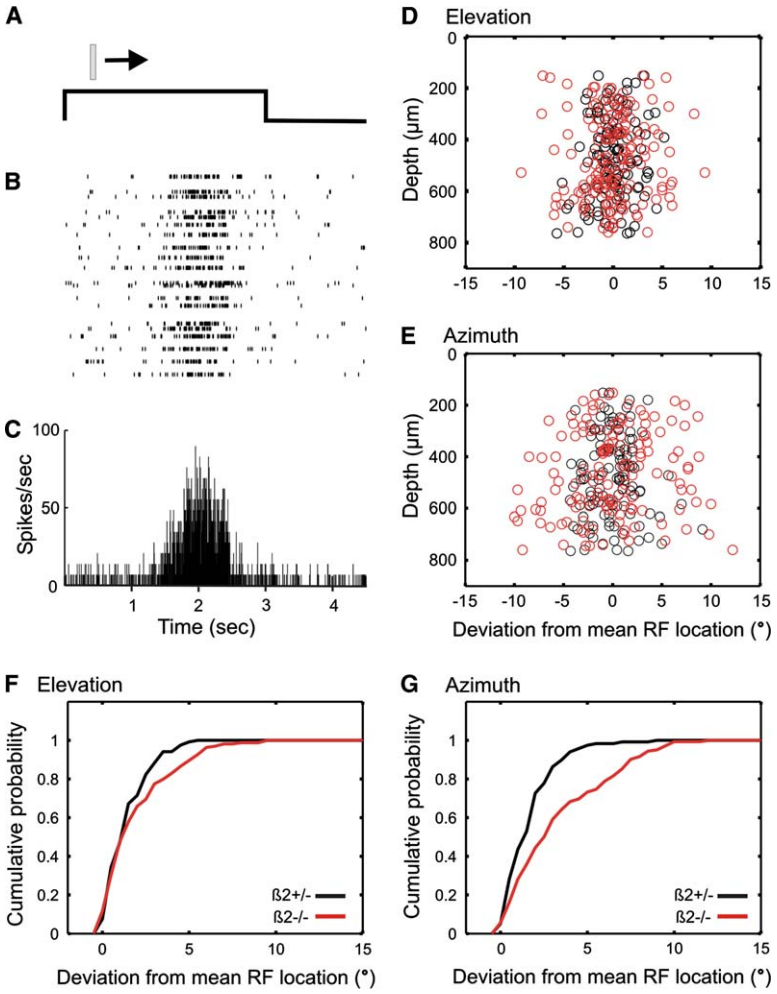

Figure 4. Precise Receptive Field Organization of Cortical Neurons Is Disrupted in $\beta2^{-/-}$ Mice

(A–C) An example of cortical spiking responses to a moving bar. (A) Each trial lasted 4.5 s. For the first 3 s, the bar swept across the stimulus monitor at a speed of 25 deg/sec. (B) Raster plots of recorded spikes for 20 repeated trials of the stimulus with the bar moving from left to right. These trials were randomly interleaved by stimuli moving in other directions: right-to-left, down-to-up, and up-to-down. (C) The PSTH of the response constructed from the 20 repeats, from which the response timing in relation to the stimulus, thus the RF location, was computed.

(D and E) Deviations of RF location of all recording sites from the mean RF location of individual penetrations are plotted as the function of recording depth for stimulus with vertically and horizontally moving bars. The $\beta2^{-/-}$ mice display a much larger scatter of RF position for both elevation and azimuth.

(F and G) Cumulative probability plots of RF deviations for elevation and azimuth. In both, the $\beta2^{-/-}$ data are significantly different from those for the $\beta2^{+/-}$ controls.

Because no systematic trend was seen in the sequence of RF positions for individual penetrations, the large variability of RF positions observed in the $\beta2^{-/-}$ mice was not an artifact of the progressive changes that would result if the recording electrodes were not completely radial.

The above experiments thus demonstrated that the cortical maps of the $\beta2^{-/-}$ mouse were defective. We further compared the defect of cortical maps with that of subcortical visual areas. Using our method of intrinsic imaging, we obtained retinotopic maps of the dLGN and superior colliculus (SC). In the animals in which we were able to image dLGN (Figure 5), the small dLGN maps of the $\beta2^{-/-}$ mice (n = 4) were of similar size and quality to those of WTs (n = 3), suggesting that the defective cortical map in the $\beta2^{-/-}$ is largely due to geniculocortical mapping errors. Because the LGN maps were too small to be compared directly to cortical maps, we instead compared SC maps to cortical maps in the same animals. Two new reports using physiological (Chandrasekaran et al., 2005) and imaging (Mrsic-Flogel et al., 2005) methods showed that the retinotopic map refinement in the SC, like that in the dLGN, is defective in the $\beta2^{-/-}$ mouse and that RF properties are clearly defective in the mutant SC (Chandrasekaran et al., 2005) but are normal in dLGN (Grubb et al., 2003; Grubb and Thompson, 2004), suggesting that the subcortical mapping defect is more severe in SC than in dLGN in the $\beta2^{-/-}$ mouse. Consistent with these two reports, we found that the SC retinotopic maps in $\beta2^{-/-}$ mice were of lower quality than the WT maps (Figure 5). More importantly, the cortical azimuth maps of $\beta2^{-/-}$ mice were much more scattered than the corresponding SC maps from the same animals (Figure 5), confirming that the altered cortical maps in the $\beta2^{-/-}$ mouse are not mere propagations of defective subcortical maps.

Pharmacologically Blocking Retinal Waves Disrupts the Precise Mapping of Geniculocortical Projections

The anatomical and functional results above demonstrate that the geniculocortical maps in the $\beta2^{-/-}$ mice are imprecise and thus defective. These mapping defects might have been caused by alterations in cholinergic signaling in the cortex or dLGN rather than by the effects of $\beta2$ deletion on retinal activity, because $\beta2$ subunit-containing nAChRs are expressed throughout the mouse brain (Zoli et al., 1998). Input from the retina during the first postnatal week is clearly necessary for the fine-scale mapping of geniculocortical projections, because these projections are normal in WT mice enucleated at P8, but are disrupted when enucleation takes place at P1 (Figure S4; and quantification below in Figure 7D). To determine whether the defect in

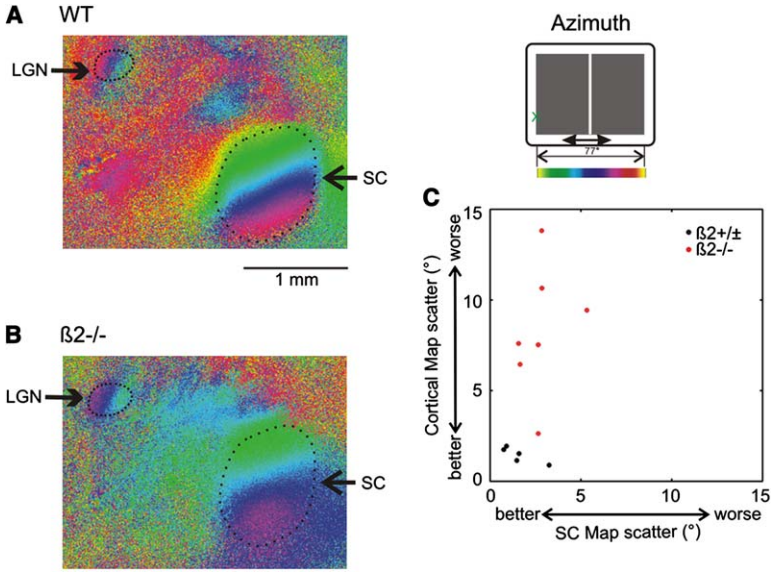

Figure 5. Cortical Retinotopic Maps Are More Defective than Subcortical Maps in $\beta2^{-/-}$ Mice

(A and B) Azimuth maps of subcortical visual areas of a WT (A) and a $\beta2^{-/-}$ mouse (B). The areas of SC and LGN are circled and labeled. Note that the dLGN map of the $\beta2^{-/-}$ mouse is no worse in quality than that of WT. Inset shows color scale for plotting maps.

(C) Scatter of cortical azimuth maps plotted against that of SC maps for individual animals. Note that the cortical maps of $\beta2^{-/-}$ mice are very much more scattered than their SC maps, in contrast to WT mice in which maps of the two areas were comparable.

geniculocortical mapping in $\beta2^{-/-}$ mice was caused by the lack of retinal waves during the first postnatal week, we disrupted the patterns of spontaneous activity in the retina of WT mice pharmacologically rather than genetically (Rossi et al., 2001). In ferrets, epibatidine, a potent nAChR agonist, abolishes the early waves of retinal activity and silences the ganglion cells that were studied by whole-cell recording (Huberman et al., 2002; Penn et al., 1998). We first examined whether epibatidine also alters retinal waves in the mouse by recording spikes from retinal ganglion cells with a multielectrode array. As expected, waves of spontaneous activity were apparent in the P4 mouse retina. These waves were disrupted by perfusion with 10 nM epibatidine (Figures 6A and 6B). Some neurons became completely silent and others had unpatterned, tonic firing

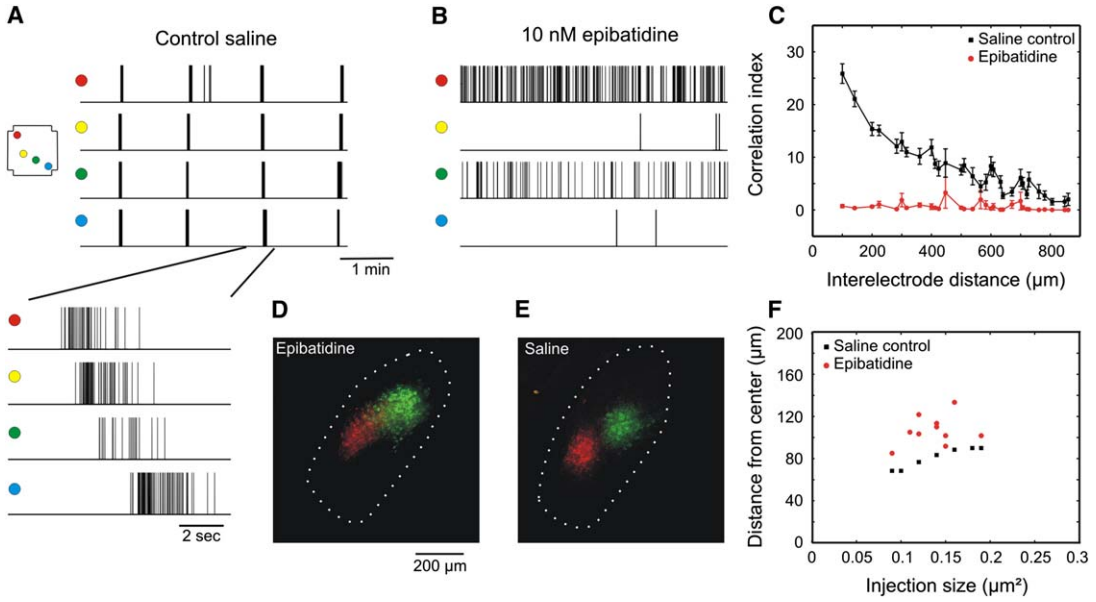

Figure 6. Pharmacologically Blocking Retinal Waves Disrupts the Precise Mapping of Geniculocortical Projections

(A) Retinal waves recorded with a multielectrode array. Spike trains of four representative neurons in a P4 WT retina are shown. A diagram of the array is shown to the left with colored circles representing the position of the four electrodes from which the spikes were recorded. One episode of the wave is shown in a finer time scale to display the details of the bursts.

(B) Spike trains of the same four neurons are shown after perfusion with 10 nM epibatidine. The patterns of retinal activity were clearly altered.

(C) Disruption of correlated spontaneous activity by epibatidine. Correlation index between retinal neurons as a function of distance between the recording electrodes. The distance-dependent correlation evident in the saline is absent in epibatidine. Error bars represent the mean ± SEM.

(D) Retrogradely labeled neurons in a dLGN section of a WT mouse that has been binocularly injected with epibatidine at P1, P3, P5, and P7. Dotted lines mark the border of the dLGN.

(E) dLGN section of a control mouse injected with saline at the same ages.

(F) The distance within which 80% of the labeled pixels were included is plotted against the injection size. Labeled areas in the dLGN were significantly larger ($p < 0.001$) in epibatidine-treated mice (107 ± 4µm) than in the saline-treated controls (81 ± 4µm).

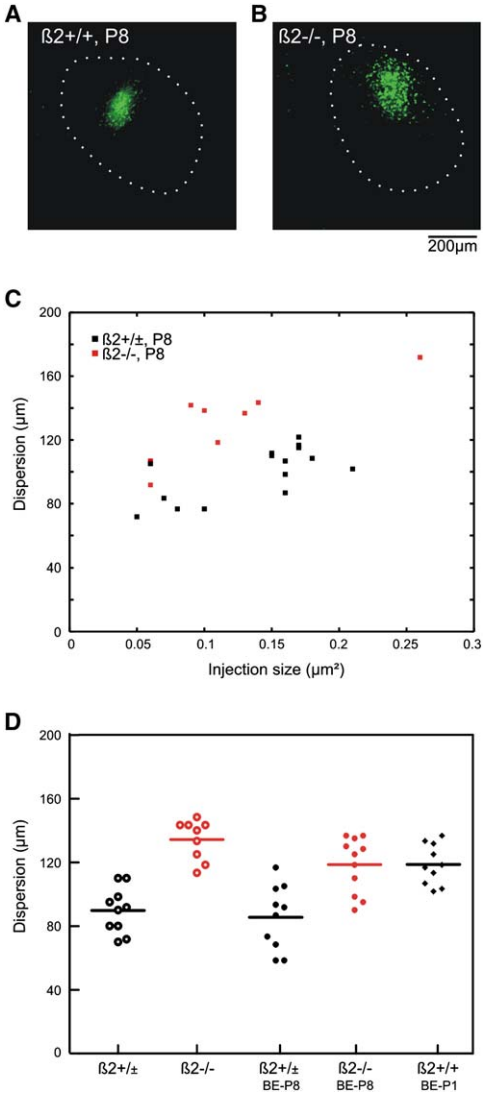

Figure 7. Geniculocortical Mapping Defect in $\beta2^{-/-}$ Mice Is Present by P8

(A and B) Retrogradely labeled neurons in the dLGN of P8 WT (A) and P8 $\beta2^{-/-}$ (B). Dotted lines mark the border of dLGN.

(C) Quantification of retrogradely labeled areas in the dLGN. The label dispersion was plotted against the injection size. The labeled areas were significantly larger in the $\beta2^{-/-}$ mice ($p < 0.01$).

(D) Quantification of labeled dLGN areas in normal and enucleated $\beta2^{+/\pm}$ (WT and heterozygous) and $\beta2^{-/-}$ mice. BE-P8 (P1), binocularly enucleated at P8 (P1).

(Figure 6B). Two hallmark features of waves in the WT retina are the highly correlated activity in near-neighbor ganglion cells and a decrease in the degree of that correlation as the distance between cells increases (Demas et al., 2003; Wong et al., 1993). With epibatidine in the saline ($n = 5$), the activity of ganglion cell pairs was uncorrelated at all distances on the array (Figure 6C), and the propagating waves were abolished.

To block retinal waves, we injected 0.5–1 nmol of epibatidine binocularly in WT mouse pups every 48 hr during their first week of postnatal life (P1, P3, P5, and P7). These mice and saline-treated littermate controls were allowed to mature to P40–P50. We analyzed the mapping of the geniculocortical projections in these mice by retrograde labeling of dLGN neurons. As we observed in the $\beta2^{-/-}$ mice, similarly sized cortical injections of the retrograde marker resulted in larger areas of labeled cells and much more overlap of the labeled areas in epibatidine-treated mice (Figures 6D–6F). Retrogradely labeled areas in the epibatidine-treated mice ($107 \pm 4\mu m$, $n = 10$) were significantly larger ($p < 0.001$) than those in the saline-treated controls ($81 \pm 4\mu m$, $n = 7$). These results demonstrate that the defective mapping of the geniculocortical projections in the $\beta2^{-/-}$ mice is due to the disruption of retinal activity during the first postnatal week.

The Geniculocortical Mapping Defects in $\beta2^{-/-}$ Mice Are Present by the End of the First Postnatal Week

Our experiments have demonstrated that the normal patterns of retinal activity in the first postnatal week are required for the precise mapping of geniculocortical projections in adult mice. The observed geniculocortical mapping defect could result directly from the disruption of retinal activity in the first week or might occur later in response to early disruption of retinogeniculate projections. To resolve the two possibilities, we examined the geniculocortical projections at P8, before the AChR-independent, glutamatergic waves appear in $\beta2^{-/-}$ mice (Bansal et al., 2000). Using the same retrograde labeling and quantification method as in adult mice, we found that the geniculocortical mapping in the $\beta2^{-/-}$ mice was already defective at P8 ($p < 0.01$; Figures 7A–7C). These results indicate that the geniculocortical mapping defect results directly from the disruption of normal activity patterns during the first week, and not from some subsequent reorganization.

The geniculocortical mapping defect in $\beta2^{-/-}$ mice observed at P8 might either become more severe or be partially rescued (Chandrasekaran et al., 2005) during later development. Because it is hard to compare the tracing results from animals of different ages, we instead performed indirect comparisons to address this question. We reasoned that any further retinotopic modification of geniculocortical mapping requires retinotopic information carried either by retinal waves in the second postnatal week or visual experience. By removing the eyes, we thus remove all retinotopic information after the date of enucleation. For adult WT mice, enucleation at P8 had little or no effect on the precision of topographic mapping (Figure S4; Figure 7D, $p > 0.05$, one-way ANOVA), indicating that the retinotopic refinement of geniculocortical projections reaches adult levels by P8. Similarly, the retrogradely labeled geniculate area in $\beta2^{-/-}$ mice was not affected by enucleation at P8 (Figure 7D, $p > 0.05$, one-way ANOVA), suggesting that no further changes of geniculocortical mapping occur after the first postnatal week. Interestingly, the labeled dLGN areas in P1-enucleated WT mice were similar to those of P8-enucleated $\beta2^{-/-}$ mice (Figure 7D, $p > 0.05$, one-way ANOVA), suggesting that lack of retinal waves during the first postnatal week may fully account for the effect of removing the eyes on geniculocortical mapping, although shrinkage of the dLGN after enucleation at P1 complicates this quantitative comparison.

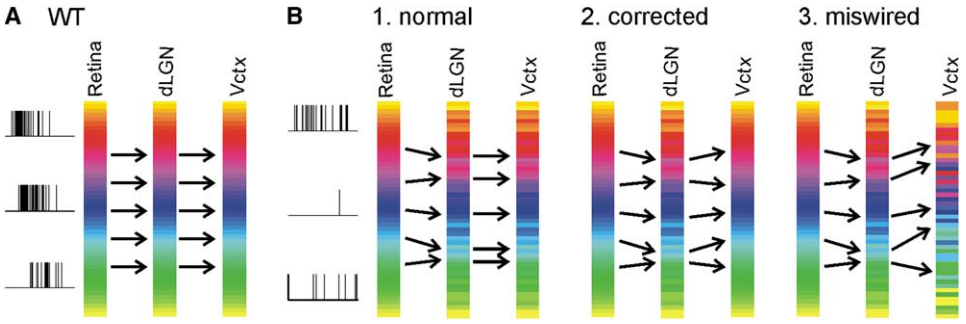

Figure 8. Retinotopic Mapping Diagrams from Retina to Cortex

(A) Topographically precise mapping of retinogeniculate and geniculocortical projections in WT mice. Color represents the range of visual field positions from nasal to temporal driving cells in retina, dLGN, and visual cortex (Vctx). Shown to the left is an episode of traveling retinal waves. (B) Three hypothetical scenarios of geniculocortical mapping when the normal activity patterns in the developing retina are disrupted, altering retinogeniculate connections. 1. normal map: geniculocortical connections do not depend on retinal activity; 2. corrected map: geniculocortical connections rearrange to compensate for retinogeniculate miswiring; 3. miswired map: geniculocortical connections are independently defective. Results demonstrate that the scenario shown in B3 is true (see Discussion).

Discussion

Precise Mapping of Geniculocortical Projections Requires Normal Patterns of Retinal Activity during the First Postnatal Week

An orderly representation of visual space in the brain is achieved in part by topographically precise connections from the dLGN to the visual cortex. In this study, we have investigated the retinal influence on mapping of the geniculocortical projection. Removing the eyes at P1, but not at P8, results in diffuse geniculocortical projections, indicating that the presence of the retina is required during the first postnatal week for the precise geniculocortical mapping. Using both mutant mice and pharmacological manipulation, we have studied whether normal patterns of retinal activity in the first postnatal week are required for the development of precise maps from the dLGN to the visual cortex.

Mice deficient in the β2 subunit of the nicotinic acetylcholine receptor do not have retinal waves in the first postnatal week, but their retinal ganglion cells maintain high-level, uncorrelated firing (McLaughlin et al., 2003b), providing a unique opportunity to study the role of correlated retinal activity in visual system development. The mapping of the retina onto its subcortical targets is known to be defective in the $\beta2^{-/-}$ mouse (Chandrasekaran et al., 2005; Grubb et al., 2003; McLaughlin et al., 2003b; Mrsic-Flogel et al., 2005; Muir-Robinson et al., 2002; Rossi et al., 2001). Before the current study, however, little was known about the geniculate map to the cortex in the absence of normal activity patterns in the developing retina.

Three different scenarios summarize how the activity might influence geniculocortical projections (Figure 8). First, the geniculocortical map might be unaffected by early retinal activity; in this case, the connections between LGN and cortex would maintain normal topographical precision (Figure 8B1), and the errors in the mapping of retinogeniculate projections (Grubb et al., 2003) would simply propagate to the visual cortex without further distortion. Such a scenario would suggest, at most, a limited role of retinal waves in the wiring of geniculocortical circuits. Our results from retrograde tracing in the $\beta2^{-/-}$ and epibatidine-treated mice demonstrate that the geniculocortical projections are clearly abnormal, thus ruling out this possibility.

The second scenario is that the map of dLGN onto the cortex might be rewired to compensate for the abnormal retinogeniculate map in $\beta2^{-/-}$ mice by bringing together in the cortex inputs from the dispersed collection of geniculate cells that receive the same retinal input (Figure 8B2). In this case, the anatomy of geniculocortical connections would be abnormal, but the functional map in the cortex would appear largely or entirely normal. Such a rewiring process might be driven by either retinal waves in the second postnatal week or visual experience after the eyes open. This second scenario is also refuted on two main grounds by our findings. First, the timing is wrong. Our anatomical studies reveal that the abnormal patterns of geniculocortical projection are fully expressed in the $\beta2^{-/-}$ mice by P8, before the noncholinergic waves of retinal activity appear. Furthermore, removing the eyes at this time has no further effect on the projection patterns in either mutant or WT mice. Second, the cortical defect is by all measures more severe than the subcortical one, not less so. Our imaging studies show that the organization of cortical retinotopy along the azimuth axis in these mice is severely defective, more so than the subcortical maps. In addition, while the retinotopic elevation map is apparently normal in the dLGN (Grubb et al., 2003), the mapping of this axis is clearly defective at the cortical level. The geniculocortical miswiring, therefore, does not represent a correction of the retinogeniculate defect.

Taken together, all of these experiments support a third scenario in which the defect in connections to the cortex in the $\beta2^{-/-}$ and epibatidine-treated mice arises independently of the retinogeniculate defect as a direct result of the disruption of activity patterns during the first postnatal week (Figure 8B3). It is known that aberrant retinogeniculate maps need not give rise to defective cortical maps. The geniculocortical maps are normal in the "Midwestern" Siamese cat and in mink and ferret of the albino series, despite abnormal retinogeniculate maps (Guillery et al., 1979; Huang and Guillery, 1985; Kaas and Guillery, 1973). In these animals, retinal

ganglion cells project aberrantly, but activity in the retina is presumed to be normal. In contrast, in $\beta2^{-/-}$ mice, the neural activity that might convey retinotopic information is not available to the geniculocortical projecting neurons due to lack of retinal waves. This results in a mapping defect in geniculocortical projections that is already present at P8.

In summary, our results are consistent with a model in which an initial coarse map of geniculocortical projections established by molecular cues (Cang et al., 2005) is normally refined by correlated activity during the period of thalamocortical ingrowth and elaboration in the first week of life. The geniculocortical map reaches adult precision by P8 and is not further refined by later retinal waves or visual experience. When the normal patterns of retinal activity are disrupted during the first week, the initial geniculocortical map fails to refine and stays diffuse into adulthood. Our results thus provide direct evidence that disrupting early spontaneous activity in the eye alters the second-stage connections from the thalamus to the cortex.

Mechanisms of Activity-Dependent Geniculocortical Mapping

What mechanisms might underlie the geniculocortical mapping defect in animals with disrupted retinal activity during the first postnatal week? In the hamster, the geniculocortical projections are not topographically organized when they first reach the subplate and deep cortical layers (Krug et al., 1998). A few days after this, when the afferent projections have arrived at layer IV, an orderly map is apparent (Krug et al., 1998). In the rat, the geniculocortical projections reach the cortical plate around P0 and layer IV around P4 (Lund and Mustari, 1977). The spatiotemporal patterns of spontaneous activity of geniculocortical axons during this period of time may influence the wiring of synaptic connections between afferent axons and cortical neurons through a Hebbian-like process (Hebb, 1949). Indeed, blocking neuronal activity by intracranial infusion of tetrodotoxin in the cat during the corresponding developmental stage alters the target selection and precision of geniculocortical projections (Catalano and Shatz, 1998). In the $\beta2^{-/-}$ and epibatidine-treated mice, the correlated activities of retinal ganglion cells are disrupted. Because the retinal input shapes the temporal patterns of correlated spontaneous activity in the dLGN and V1 during development (Chiu and Weliky, 2001; Mooney et al., 1996; Weliky and Katz, 1999), the altered timing of activity in dLGN and V1 when retinal waves are disrupted may thus result in geniculocortical mapping errors.

In the $\beta2^{-/-}$ mouse, at least 60% of retinal ganglion cells are spontaneously active, and these cells maintain high levels of uncorrelated activity (McLaughlin et al., 2003b). Although the percentage of active ganglion cells is certainly underestimated by the method used, which fails to detect activity in cells that fire only individual spikes rather than bursts (McLaughlin et al., 2003b), some populations of ganglion cells may indeed be silent in the $\beta2^{-/-}$ mouse, as well as in the epibatidine-treated retinas. In our study in vitro, some ganglion cells treated with 10 nM epibatidine became silent, consistent with findings in ferrets (Penn et al., 1998) and rabbits (Kittila and Massey, 1997). Because the concentration of epibatidine in vivo and the effect of prolonged exposure to epibatidine on ganglion cell activity are not known, the precise activity level of ganglion cells in the injected retinae is uncertain. It is therefore possible that the minority of silent ganglion cells, instead of active cells with altered patterns, is responsible for the mapping errors of retinogeniculate (Grubb et al., 2003) and retinocollicular (Chandrasekaran et al., 2005) projections in the $\beta2^{-/-}$ and epibatidine-treated mice. Such a possibility, however, is unlikely for the geniculocortical mapping defects. Before eyes open, each geniculate cell receives inputs from a large number of ganglion cells (Chen and Regehr, 2000; Jaubert-Miazza et al., 2005) and would therefore not be silent even if some of the inputs were. In fact, even when all of the retinal inputs are removed at a similar developmental stage in ferrets, the geniculate cells are spontaneously active (Chiu and Weliky, 2001; Weliky and Katz, 1999). Consequently, the effect of the silent ganglion cells on the firing patterns of geniculate cells is likely to be small. It is more probable that the patterns of the active ganglion cells shape the dLGN firing patterns, which, due to their lack of local correlation, lead to the mapping defect of geniculocortical projections.

We have interpreted the defects in geniculocortical mapping in the $\beta2^{-/-}$ mouse as resulting directly from the altered pattern of neural activity in the dLGN and cortex during the first week of life. However, it is also possible that the altered retinal activity patterns act indirectly to produce abnormal expression of molecular guidance cues in the dLGN. Normal patterns of spontaneous activity are indeed required for the expression of specific guidance molecules in spinal motoneurons (Hanson and Landmesser, 2004). If this were also the case in the visual pathway, a change in molecular guidance cues expressed in the dLGN in the absence of retinal waves might account for both retinogeniculate and geniculocortical mapping errors. Equally conceivably, the ability of projecting axons to "read out" the gradient of guidance molecules could be diminished by the altered activity patterns, thereby producing mapping errors. In this light, it is interesting that the geniculocortical projections in the $\beta2^{-/-}$ mouse are more severely affected along the nasotemporal axis than along the dorsoventral axis. Similar asymmetric mapping errors have been observed for the retinogeniculate (Grubb et al., 2003) and retinocollicular (Chandrasekaran et al., 2005) projections in the $\beta2^{-/-}$ mouse. Because no preference for one axis of the retina over the other has been observed for the traveling retinal waves, it is attractive to hypothesize that the guidance molecules for the nasotemporal axis, such as ephrin-As (Feldheim et al., 2000; Cang et al., 2005), may be preferentially altered in the absence of normal patterns of activity.

Comparisons with Ocular Dominance Column Development

The establishment of ocular dominance columns (ODCs) has served as a model system for studying thalamocortical patterning and cortical development (Feller and Scanziani, 2005). It has been proposed that molecular guidance cues mediate the establishment of ODCs, based on studies in enucleated ferrets suggesting that retinal input is not needed for the initial segregation of

geniculocortical projections into ODCs (Crowley and Katz, 1999, 2000). While mice do not have ODCs, our enucleation experiments do demonstrate that retinal input during the first postnatal week is required for the topographically precise mapping of geniculocortical projections. Recent studies are consistent with the idea that spontaneous activity may also play an important role for the formation of ODCs, because the dLGN and visual cortex maintain correlated (though abnormal) bursting activities even after retinal inputs are severed (Chiu and Weliky, 2001; Weliky and Katz, 1999). These sustained bursts in enucleated animals are appropriate for driving activity-dependent segregation of geniculocortical afferents (Miller et al., 1989), which depends on large-scale correlations within geniculate laminae. On the other hand, precise timing of the correlated spontaneous activity could be critical for the establishment and refinement of precise retinotopic mapping (Butts and Rokhsar, 2001). This signal about the spatial origin of afferent axons would be missing in the absence of input from the eyes. It is therefore possible that segregation of eye-specific geniculocortical afferents to form ODCs may require different features of retinal waves than does the formation of a precise retinotopic map. Activity sufficient for the former appears to be present in the dLGN of enucleated animals, but not for the latter.

Implications for Cortical Development

Until very recently, studies of activity-dependent plasticity in the developing visual cortex have focused on the critical period of susceptibility to the effect of monocular occlusion beginning near the end of the third week of life. This time corresponds to a phase in cortical development very different from the critical period of the primary somatosensory "barrel" cortex in the first postnatal week (Fox, 1992). A few studies have shown visual cortical circuit changes that depend on eye opening at the end of the second week (Maffei et al., 2004; Yoshii et al., 2003); this plasticity is presumably mediated by the consequent changes in retinal activity. We now provide evidence that retinal activity during the first week of life is essential for organizing precise connections to the visual cortex. This form of activity-dependent plasticity, which aids in the establishment of a precise topographic order, appears likely to correspond to the critical period for barrel cortex. It takes place at the same point in the life history of the cells and serves a similar function. In both systems, a defect in the sensory periphery does not abolish thalamocortical topography, but instead prevents it from refining to its normal precision. The role now revealed for patterns of spontaneous neural activity in the establishment of maps during the initial ingrowth and elaboration of connections to the cortex may be general and may account for abnormalities in human development.

Experimental Procedures

Animals

Mice with heterozygous alleles of the β2 subunit of the nicotinic acetylcholine receptor ($\beta2^{+/-}$) were kindly provided by Dr. Art Beaudet from Baylor College of Medicine (Xu et al., 1999). These mice were bred after backcrossing onto a C57Bl/6 strain for many generations. We maintained colonies of heterozygous ($\beta2^{+/-}$) and homozygous ($\beta2^{-/-}$) mice from these breeding pairs. The genotypes were determined according to the published protocol (Xu et al., 1999). Additional control experiments were performed on age-matched wild-type C57Bl/6 mice (Charles River Labs).

Physiological Preparation and Functional Imaging of Retinotopic Maps

All surgical procedures were approved by the University of California, San Francisco Committee on Animal Research. To image mouse cortical retinotopy, we followed the method developed by Kalatsky and Stryker (Kalatsky and Stryker, 2003). Briefly, adult mice between 2 and 6 months of age were anesthetized with urethane (1.0 g/kg i.p.) supplemented by chlorprothixene (0.2 mg/mouse i.m.). Atropine (5 mg/kg) and dexamethasone (0.2 mg/mouse) were injected subcutaneously. A tracheotomy was performed, and a craniotomy was made over the visual area of the left hemisphere; the dura mater was left intact. For survival experiments to retrogradely label dLGN neurons, the animals were anesthetized using 1%–2% isoflurane in O_2, and no tracheotomy was performed. To image subcortical visual areas, the overlying cortex was aspirated, thereby exposing SC and dLGN.

Optical images of cortical intrinsic signal were obtained using a Dalsa 1M30 CCD camera (Dalsa, Waterloo, Canada) controlled by custom software. The surface vascular pattern or intrinsic signal images were visualized with illumination wavelengths set by a green (546 ± 10 nm) or red (610 ± 10 nm) interference filter, respectively. After acquisition of a surface image, the camera was focused 600 μm below the pial surface. An additional red filter was interposed between the brain and the CCD camera, and intrinsic signal images were acquired at the rate of 7.5 fps and were stored as 512 × 512 pixel images.

A high refresh rate monitor (Nokia Multigraph 445X, 1024 × 768 pixels, 120 Hz) was placed 25 cm away, to the right (contralateral to the hemisphere being imaged), with its left edge approximately aligned to the animal. Drifting thin bars (2° wide and full-screen length) were generated by a Matrox G450 board (Matrox Graphics, Inc., Quebec, Canada). The spatial frequency of the drifting bar was 1 cycle/80 degrees, and the temporal frequency was 1 cycle/8 s or 1 cycle/6 s. Animals were presented with thin bars drifting along the vertical or horizontal axes in order to stimulate the constant lines of elevation or azimuth, respectively. By extracting the optical signal at the stimulus frequency, we computed the response magnitudes and timing in reference to the stimulus cycle, which can then be converted to the location of the visual field. The absolute phase maps were then calculated by the method of "phase reversal" (Kalatsky and Stryker, 2003).

Analysis of Retinotopic Maps

We used two measures to compare cortical maps. First, we determined the maximum magnitude of optical response (expressed as fractional change in reflectance × 10^4) from the absolute map. Second, to assess map quality, we selected the most responsive area within the primary visual cortex (V1) to compare the visual field positions of these pixels with those of their neighbors. Specifically, we used the elevation map to select the response area, because the azimuth maps of $\beta2^{-/-}$ mice are very weak. The 20,000 pixels (1.60 mm^2 of cortical space) that had the greatest response magnitude in the elevation maps were selected. For each of these pixels, we calculated the difference between its position and the mean position of its surrounding 25 pixels. For maps of high quality, the position differences are quite small because of smooth progression. The standard deviation of the position difference was then used as an index of map quality. The quality of SC maps was similarly analyzed, using 5,000 pixels due to the smaller area of SC. Note that the compression of the SC map relative to the V1 map would cause any artifactual scatter that resulted from the measurement procedure to be greater in SC than in V1, ensuring that the greater measured scatter in $\beta2^{-/-}$ V1 is an underestimate.

Multiunit Recording of Cortical Neurons and Analysis of Receptive Fields

Guided by the optical maps, we recorded multiunit activity from V1 with 10 MΩ microelectrodes (Frederick Haer Company, Bowdoinham, ME). For each animal, three to six penetrations were made perpendicular to the pial surface across V1, and three to seven sites

(>50 μm apart) were recorded in each penetration. The spikes were acquired using a System 3 workstation (Tucker Davis Technologies, FL) and analyzed using Matlab (The Mathworks, MA).

Single drifting bars 5° in width and 80° in length at the speed of 25°/sec were used to drive cortical cells. In each trial, the drifting bar was presented in four directions—rightward, leftward, upward, and downward—in a random sequence. Twenty to thirty of such trials were repeated to construct a peristimulus time histogram (PSTH) for each stimulus direction, using 5 ms bins. The PSTH was subsequently smoothed using a 10 ms window. The mean rate (R_b) and standard deviation (Std_b) of background firing activity were calculated from the period of PSTH when no stimulus was presented. A threshold was calculated as $R_b + 3 * Std_b$, and the bins in the PSTH above the threshold were used to calculate the mean timing weighted by their firing rate. Separately for each of the four directions of movement, the RF location was determined by converting the timing to position on the stimulus monitor, and the mean RF location of each penetration was calculated from all of the recording sites. The RF deviation of each recording site from the mean RF position was used to assay the precision of cortical RF organization.

Retrograde Labeling of Thalamocortical Projections and Image Analysis

Cholera toxin subunit B (CTB) conjugated to Alexa Fluor (Molecular Probes, OR), CTB-488 (green), and CTB-594 (red) were injected into the cortex, guided by the retinotopic maps or stereotaxic coordinates to retrogradely label dLGN neurons. A small amount of 2 mg/ml solution of each CTB in PBS was injected by Nanoject (Drummond Scientific Company, PA), using a glass pipette with a 20–30 μm tip opening. The Nanoject was set to inject 32.2 nl of the dye (18.4 nl for P8 mice), but small variations in injection volume were unavoidable. Mice were sacrificed and intercardially perfused with 4% paraformaldehyde in PBS 48 hr later. The brains were fixed overnight before sectioning coronally at 100 μm using a vibratome (Lancer, MO). Images of the dLGN and injection sites in the cortex were captured using a confocal microscope (Biorad 1024, CA).

To analyze the patterns of retrogradely labeled cells in the dLGN, we first calculated the background signal as the mean signal of an area within the dLGN where no labeled cells were seen. The image was then thresholded separately for each color at the level of 1.5 times the background. (A wide range of threshold from 1.2 to 1.8× was tested and similar results were obtained.) We then calculated the position of the center of mass for all of the labeled pixels within the dLGN. The percentage of labeled pixels within the dLGN as a function of the distance from the center was then computed. The above procedure was repeated for all sections of the dLGN (six to seven 100 μm sections per animal). The sections at the rostral and caudal ends were excluded due to the small number of labeled pixels. Finally, we calculated the mean of the percentage of labeled pixels in all sections of each animal. To quantify the differences between the control and $\beta2^{-/-}$ mice, we used the radius of the circle within which 80% of the labeled pixels were found to represent the degree of the dispersion.

To calculate the actual size of injection, we reconstructed the injection sites from the 100 μm coronal sections. From each section, we measured the width of the dye at the level of layer IV, i.e., 400 μm from the pial surface. The area of injection in this section is then the product of the width of the dye and the section thickness (100 μm). The total area was then calculated as the sum of all sections.

Multielectrode Extracellular Recording from Retina

P4 WT mice were sacrificed by decapitation. Retinal dissection was performed in a bicarbonate-based extracellular saline under normal room illumination. The saline consisted of: 124 mM NaCl, 2.5 mM KCl, 2 mM $CaCl_2$, 2 mM $MgCl_2$, 1.25 mM NaH_2PO_4, 26 mM $NaHCO_3$, and 22.2 mM glucose; the pH was maintained at 7.3–7.4 by bubbling with a mixture of 95%O_2/5% CO_2. The retina was placed in a multielectrode chamber (MEA-60 system; MultiChannel Systems, Germany) ganglion cell-side down. Retinas were perfused for 30 min at room temperature and then for 30 min at 34°C before recordings were started, and the temperature was maintained at 34°C throughout the recordings.

Multielectrode data were analyzed using OfflineSorter software (v.1.3; Plexon Inc., TX) as described previously (Tian and Copenhagen, 2003). Correlation indices of these units, as described in Wong et al. (1993), were calculated with IGOR Pro (v.4.0; WaveMetrics, OR) using custom macros. The correlation index for a given pair of neurons indicates the fold increase of the firing rate of one neuron within a given time window of a spike from the other neuron. It was calculated using the number of spikes from one neuron that were detected within the time window (100 ms) of a spike from the other neuron. This value was scaled to the mean firing rate of the first neuron and the firing rate of the other neuron during the time window. The correlation index increases with the likelihood of the simultaneous firing of the two neurons (Demas et al., 2003).

In Vivo Intravitreous Application of Epibatidine

Every 48 hr from P1 to P7, mice were anesthetized, and 0.5–1 μl of 1 mM epibatidine (Sigma, MO) in sterile saline, or sterile saline alone, was injected intravitreously into both eyes. We confirmed that the effects of epibatidine injections were limited to the eye and did not reach the CNS via the circulation, by systemic administration of the same dose in other animals, which produced CNS signs within 3 min. Eye injections at P1 and P3 were performed through the intact eyelids, and at P5 and P7 the eyelids were cut open. A 33G needle attached to a Hamilton (Reno, NV) microsyringe was used to inject the solution at the rate of about 1 μl/min into the vitreous humor at the ora serrata. The needle is withdrawn after holding it in place for 30 s to 1 min. The animals were allowed to survive to P40–P50 before the dLGN neurons were retrogradely labeled with CTBs. Functional imaging was not performed in these animals, and the CTBs were injected at the same stereotaxic coordinates as in the mice defined by imaging. The retinal morphology was examined in both epibatidine- and saline-treated mice to confirm that their retinas were not damaged by the intravitreous injections.

Data Analysis

The statistical test used was Student's t test and the results were expressed as the mean ± standard error, unless otherwise indicated.

Supplemental Data

Supplemental Data include four figures and can be found with this article online at http://www.neuron.org/cgi/content/full/48/5/797/DC1/.

Acknowledgments

We thank Dr. Art Beaudet, for making this study possible by providing heterozygous β2 mice and Dr. Marla Feller, for providing homozygous β2 mice for our pilot experiments and for comments on the manuscript. We also thank Liz Hawkes, for genotyping; Ann Schreiber, for sectioning; and Drs. David Feldheim, Patrick McQuillen, Andrew Huberman, Andrew Tan, and members of the Stryker lab, for discussions. Our work is supported by N.I.H. grants to M.P.S. and D.R.C. J.C. is an Aventis Pharmaceuticals Fellow of the Life Sciences Research Foundation. Additional support was provided by That Man May See, Research to Prevent Blindness, and the Knights Templar Eye Foundation.

Received: April 25, 2005
Revised: August 12, 2005
Accepted: September 13, 2005
Published: December 7, 2005

References

Bansal, A., Singer, J.H., Hwang, B.J., Xu, W., Beaudet, A., and Feller, M.B. (2000). Mice lacking specific nicotinic acetylcholine receptor subunits exhibit dramatically altered spontaneous activity patterns and reveal a limited role for retinal waves in forming ON and OFF circuits in the inner retina. J. Neurosci. *20*, 7672–7681.

Butts, D.A., and Rokhsar, D.S. (2001). The information content of spontaneous retinal waves. J. Neurosci. *21*, 961–973.

Cang, J., Kaneko, M., Yamada, J., Woods, G., Stryker, M.P., and Feldheim, D.A. (2005). Ephrin-As guide the formation of functional maps in the visual cortex. Neuron *48*, 577–589.

Catalano, S.M., and Shatz, C.J. (1998). Activity-dependent cortical target selection by thalamic axons. Science *281*, 559–562.

Chandrasekaran, A.R., Plas, D.T., Gonzalez, E., and Crair, M.C. (2005). Evidence for an instructive role of retinal activity in retinotopic map refinement in the superior colliculus of the mouse. J. Neurosci. *25*, 6929–6938.

Chen, C., and Regehr, W.G. (2000). Developmental remodeling of the retinogeniculate synapse. Neuron *28*, 955–966.

Chiu, C., and Weliky, M. (2001). Spontaneous activity in developing ferret visual cortex in vivo. J. Neurosci. *21*, 8906–8914.

Crowley, J.C., and Katz, L.C. (1999). Development of ocular dominance columns in the absence of retinal input. Nat. Neurosci. *2*, 1125–1130.

Crowley, J.C., and Katz, L.C. (2000). Early development of ocular dominance columns. Science *290*, 1321–1324.

Demas, J., Eglen, S.J., and Wong, R.O. (2003). Developmental loss of synchronous spontaneous activity in the mouse retina is independent of visual experience. J. Neurosci. *23*, 2851–2860.

Eglen, S.J., Demas, J., and Wong, R.O. (2003). Mapping by waves. Patterned spontaneous activity regulates retinotopic map refinement. Neuron *40*, 1053–1055.

Feldheim, D.A., Kim, Y.I., Bergemann, A.D., Frisen, J., Barbacid, M., and Flanagan, J.G. (2000). Genetic analysis of ephrin-A2 and ephrin-A5 shows their requirement in multiple aspects of retinocollicular mapping. Neuron *25*, 563–574.

Feller, M.B., and Scanziani, M. (2005). A precritical period for plasticity in visual cortex. Curr. Opin. Neurobiol. *15*, 94–100.

Feller, M.B., Wellis, D.P., Stellwagen, D., Werblin, F.S., and Shatz, C.J. (1996). Requirement for cholinergic synaptic transmission in the propagation of spontaneous retinal waves. Science *272*, 1182–1187.

Fox, K. (1992). A critical period for experience-dependent synaptic plasticity in rat barrel cortex. J. Neurosci. *12*, 1826–1838.

Galli, L., and Maffei, L. (1988). Spontaneous impulse activity of rat retinal ganglion cells in prenatal life. Science *242*, 90–91.

Godement, P., Salaun, J., and Imbert, M. (1984). Prenatal and postnatal development of retinogeniculate and retinocollicular projections in the mouse. J. Comp. Neurol. *230*, 552–575.

Grubb, M.S., and Thompson, I.D. (2004). Visual response properties in the dorsal lateral geniculate nucleus of mice lacking the beta2 subunit of the nicotinic acetylcholine receptor. J. Neurosci. *24*, 8459–8469.

Grubb, M.S., Rossi, F.M., Changeux, J.P., and Thompson, I.D. (2003). Abnormal functional organization in the dorsal lateral geniculate nucleus of mice lacking the beta 2 subunit of the nicotinic acetylcholine receptor. Neuron *40*, 1161–1172.

Guillery, R.W., Oberdorfer, M.D., and Murphy, E.H. (1979). Abnormal retino-geniculate and geniculo-cortical pathways in several genetically distinct color phases of the mink (Mustela vison). J. Comp. Neurol. *185*, 623–655.

Hanson, M.G., and Landmesser, L.T. (2004). Normal patterns of spontaneous activity are required for correct motor axon guidance and the expression of specific guidance molecules. Neuron *43*, 687–701.

Hebb, D.O. (1949). The organization of behavior: a neuropsychological theory (New York: Wiley).

Huang, K., and Guillery, R.W. (1985). A demonstration of two distinct geniculocortical projection patterns in albino ferrets. Brain Res. *352*, 213–220.

Huberman, A.D., Stellwagen, D., and Chapman, B. (2002). Decoupling eye-specific segregation from lamination in the lateral geniculate nucleus. J. Neurosci. *22*, 9419–9429.

Huberman, A.D., Wang, G.Y., Liets, L.C., Collins, O.A., Chapman, B., and Chalupa, L.M. (2003). Eye-specific retinogeniculate segregation independent of normal neuronal activity. Science *300*, 994–998.

Jaubert-Miazza, L., Green, E., Lo, F., Bui, K., Mills, J., and Guido, W. (2005). Structural and functional composition of the developing retinogeniculate pathway in the mouse. Vis. Neurosci. *22*, 661–676.

Kaas, J.H., and Guillery, R.W. (1973). The transfer of abnormal visual field representations from the dorsal lateral geniculate nucleus to the visual cortex in Siamese cats. Brain Res. *59*, 61–95.

Kalatsky, V.A., and Stryker, M.P. (2003). New paradigm for optical imaging: temporally encoded maps of intrinsic signal. Neuron *38*, 529–545.

Katz, L.C., and Shatz, C.J. (1996). Synaptic activity and the construction of cortical circuits. Science *274*, 1133–1138.

Kittila, C.A., and Massey, S.C. (1997). Pharmacology of directionally selective ganglion cells in the rabbit retina. J. Neurophysiol. *77*, 675–689.

Krug, K., Smith, A.L., and Thompson, I.D. (1998). The development of topography in the hamster geniculo-cortical projection. J. Neurosci. *18*, 5766–5776.

Lund, R.D., and Mustari, M.J. (1977). Development of the geniculocortical pathway in rats. J. Comp. Neurol. *173*, 289–306.

Maffei, A., Nelson, S.B., and Turrigiano, G.G. (2004). Selective reconfiguration of layer 4 visual cortical circuitry by visual deprivation. Nat. Neurosci. *7*, 1353–1359.

McLaughlin, T., Hindges, R., and O'Leary, D.D. (2003a). Regulation of axial patterning of the retina and its topographic mapping in the brain. Curr. Opin. Neurobiol. *13*, 57–69.

McLaughlin, T., Torborg, C.L., Feller, M.B., and O'Leary, D.D. (2003b). Retinotopic map refinement requires spontaneous retinal waves during a brief critical period of development. Neuron *40*, 1147–1160.

Meister, M., Wong, R.O., Baylor, D.A., and Shatz, C.J. (1991). Synchronous bursts of action potentials in ganglion cells of the developing mammalian retina. Science *252*, 939–943.

Miller, K.D., Keller, J.B., and Stryker, M.P. (1989). Ocular dominance column development: analysis and simulation. Science *245*, 605–615.

Mooney, R., Penn, A.A., Gallego, R., and Shatz, C.J. (1996). Thalamic relay of spontaneous retinal activity prior to vision. Neuron *17*, 863–874.

Mrsic-Flogel, T.D., Hofer, S.B., Creutzfeldt, C., Cloez-Tayarani, I., Changeux, J.P., Bonhoeffer, T., and Hubener, M. (2005). Altered map of visual space in the superior colliculus of mice lacking early retinal waves. J. Neurosci. *25*, 6921–6928.

Muir-Robinson, G., Hwang, B.J., and Feller, M.B. (2002). Retinogeniculate axons undergo eye-specific segregation in the absence of eye-specific layers. J. Neurosci. *22*, 5259–5264.

Penn, A.A., Riquelme, P.A., Feller, M.B., and Shatz, C.J. (1998). Competition in retinogeniculate patterning driven by spontaneous activity. Science *279*, 2108–2112.

Rossi, F.M., Pizzorusso, T., Porciatti, V., Marubio, L.M., Maffei, L., and Changeux, J.P. (2001). Requirement of the nicotinic acetylcholine receptor beta 2 subunit for the anatomical and functional development of the visual system. Proc. Natl. Acad. Sci. USA *98*, 6453–6458.

Shatz, C.J., and Stryker, M.P. (1988). Prenatal tetrodotoxin infusion blocks segregation of retinogeniculate afferents. Science *242*, 87–89.

Stryker, M.P., and Harris, W.A. (1986). Binocular impulse blockade prevents the formation of ocular dominance columns in cat visual cortex. J. Neurosci. *6*, 2117–2133.

Tian, N., and Copenhagen, D.R. (2003). Visual stimulation is required for refinement of ON and OFF pathways in postnatal retina. Neuron *39*, 85–96.

Weliky, M., and Katz, L.C. (1999). Correlational structure of spontaneous neuronal activity in the developing lateral geniculate nucleus in vivo. Science *285*, 599–604.

Wong, R.O., Meister, M., and Shatz, C.J. (1993). Transient period of correlated bursting activity during development of the mammalian retina. Neuron *11*, 923–938.

Xu, W., Orr-Urtreger, A., Nigro, F., Gelber, S., Sutcliffe, C.B., Armstrong, D., Patrick, J.W., Role, L.W., Beaudet, A.L., and De Biasi, M. (1999). Multiorgan autonomic dysfunction in mice lacking the beta2 and the beta4 subunits of neuronal nicotinic acetylcholine receptors. J. Neurosci. *19*, 9298–9305.

Yoshii, A., Sheng, M.H., and Constantine-Paton, M. (2003). Eye opening induces a rapid dendritic localization of PSD-95 in central visual neurons. Proc. Natl. Acad. Sci. USA *100*, 1334–1339.

Zoli, M., Lena, C., Picciotto, M.R., and Changeux, J.P. (1998). Identification of four classes of brain nicotinic receptors using beta2 mutant mice. J. Neurosci. *18*, 4461–4472.